Crimson Publishers
Wings to the Research

Research Article

HDI Based Poly(Urethane Methacrylate) Nanocomposites Containing Nano$CaCO_3$: Preparation and Properties

Praveen S, Santhana Gopala Krishnan P*, Purushothaman M and Nayak SK

Department of Plastics Technology, Central Institute of Petrochemicals Engineering and Technology (CIPET), Institute of Petrochemicals Technology (IPT), Chennai, India

ISSN: 2770-6613

***Corresponding author:** P Santhana Gopala Krishnan, Department of Plastics Technology, Central Institute of Petrochemicals Engineering and Technology (CIPET), Institute of Petrochemicals Technology (IPT), TVK Industrial Estate, Chennai, India

Submission: February 16, 2021

Published: March 23, 2021

Volume 1 - Issue 5

How to cite this article: Praveen S, Santhana Gopala Krishnan P, Purushothaman M, Nayak SK. HDI Based Poly(Urethane Methacrylate) Nanocomposites Containing Nano$CaCO_3$: Preparation and Properties. Polymer Sci Peer Rev J. 1(5). PSPRJ. 000522. 2021.
DOI: 10.31031/PSPRJ.2021.01.000522

Abstract

In situ polymerization technique was used to prepare poly(urethane methacrylate) nanocomposite sheets, using Poly(Ethylene Glycol) (PEG-400), 1,6-Hexamethylene Diisocyanate (HDI), 2-hydroxyethyl methacrylate (HEMA), calcium carbonate ($CaCO_3$) as nanofiller and Methyl Methacrylate (MMA) as reactive diluent. Fourier Transform Infrared (FT-IR) and Wide-Angle X-Ray Diffraction (WAXD) studies confirmed the incorporation of nano$CaCO_3$ in polymer matrix. Density of the nanocomposites exhibited loose structure of materials. Tensile and flexural strength as well as modulus, hardness and abrasion resistance of nanocomposites increased with increase in nano$CaCO_3$ content. But impact strength decreased with increase in nano$CaCO_3$ content up to 1% and there after it levels off. Scanning Electron Microscopic (SEM) images confirmed the uniform distribution of nano$CaCO_3$ in composites up to 2% (w/w) of nano$CaCO_3$. SEM images of abraded samples indicated micro ploughing occurred during wearing. All nanocomposites were found to be stable up to 200 °C and having two-step thermal degradation in nitrogen atmosphere.

Keywords: Thermoset; Preparation; Mechanical and thermal properties

Abbreviations: WAXD: Wide-Angle X-Ray Diffraction; FT-IR: Fourier Transform Infra-Red; SEM: Scanning Electron Microscopic; HDI: Hexamethylene Di Isocyanate; MMA: Methyl Meth Acrylate; PUMA: Poly Urethane Meth Acrylate

Introduction

Prepolymer of polyurethane usually reacted with (meth)acrylic monomers in order to improve the Poly Urethane (PU) properties like chemical resistance, tensile, flexural and impact strengths and adhesion [1-3]. Such materials are used in UV curable coatings [4], dye sensitized solar cells [5], shape memory/ recovery [6], corrosion protection [7], microfluidic devices [8], 3D printing [9] and negative photoresists [10]. But inferior properties such as barrier, abrasion, wear resistance, fire retardancy and thermal stability, limits the applications of PU. These properties can be substantially improved by inorganic fillers in the form of micron or nano size which has received much attention to make composites using polymer matrix. Nanofillers such as zinc sulphides [11], silica [12], graphene oxide [13], zinc oxide [14], gold and silver [15] were used to prepare PUMA nanocomposites and their properties are well documented in literature. Such nanocomposites were made by different types of methods like *in situ* polymerization, chemical reduction, solution blending, melt blending and frontal polymerization. Cost effectiveness and fillers abundance were considered to make nanocomposites with good mechanical and thermal properties. $CaCO_3$ has been widely used in industries because of its easy availability, low cost, non-toxicity and non-abrasiveness. Polymer dispersed with nano$CaCO_3$ provides excellent mechanical properties due to the high surface area to volume ratio. Literature survey reveals that the different types [16] and sizes [17] of $CaCO_3$ were widely used in polymers to improve their mechanical and thermal properties. Polymers such as $CaCO_3$ filled polypropylene [18], polystyrene [19], Poly(Methyl Methacrylate) (PMMA) [20], acrylonitrile butadiene styrene [21], polyacrylamide [22], polyimide [23], butadiene rubber [24], epoxy [25], unsaturated polyester [26], poly(lactic acid) [27], polycaprolactum [28], chitosan [29], and gluten [30] were reported. Such nanocomposites find applications requiring enhanced non-abrasiveness and excellent mechanical properties. But limited work has been reported for PUMA containing $CaCO_3$ composites.

In our previous work, Polymeric Diphenylmethane Diisocyanate (PMDI) based PUMA/ $CaCO_3$ nanocomposite was reported [31]. In continuation to the previous work, we prepared

1,6-Hexamethylene Diisocyanate (HDI) based PUMA matrix with different weight percentage of nanoCaCO$_3$ composites. To the best of our knowledge no work has been reported for preparation of PUMA using HDI, PEG 400, HEMA, MMA and nanoCaCO$_3$ by *in situ* polymerization. The changes in their mechanical, optical, surface and thermal properties were explained on the basis of its chemical structure and composition.

Experimental

Materials

Poly(Ethylene Glycol) (PEG 400) was procured from Qualigen Fine Chemicals (Chennai, India). 1,6-Hexamethylene Diisocyanate (HDI), 2-Hydroxyethyl Methacrylate (HEMA) and stannous octoate were obtained from Sigma Aldrich. Methyl Methacrylate (MMA) was obtained from s.d. fine chemicals (India). 2,2′-Azobisisobutyronitrile (AIBN, Spectrochem) was recrystallized twice from chloroform. The commercial nanoCaCO$_3$ (average particle size of 65nm) was provided by Reena Organics India Pvt. Ltd. All other chemicals were used as received.

Preparation of prepolymer and nanocomposites

PEG 400 (55mmol, 22g), HDI (110mmol, 18.5g) and HEMA (110mmol, 14.3g) were used to prepare pre-polymer of Urethane Methacrylate (UMA). PEG 400, HEMA and few drops of stannous octoate were taken in a 500mL three necked round-bottomed flask fitted with a mechanical stirrer and nitrogen inlet. MMA was used as reactive diluent. The reaction mixture was cooled using ice cubes and then HDI was added drop wise for about 3h. The reaction is shown in Figure 1. After the completion of HDI addition, the reaction was carried out at ambient temperature in nitrogen atmosphere. Periodically, the reaction was monitored by FT-IR spectroscopy to confirm the disappearance of isocyanate peak at 2250cm^{-1}. Reaction was completed in about 36h. The above procedure was followed for the preparation of PUMA-CaCO$_3$ nanocomposites. Initially, nanoCaCO$_3$ was dispersed in HEMA for 30min at room temperature using an ultrasonicator. Frequency and amplitude of ultrasonicator are 33±3kHz and 100%, respectively. Various nanocomposites were made by changing the nanoCaCO$_3$ content ranging from 0.5, 1.0, 1.5 and 2.0 % (w/w). It was observed that nanoCaCO$_3$ begun to settle in HEMA when the concentration was increased above 2%. So, further addition of nanoCaCO$_3$ in HEMA was not carried out.

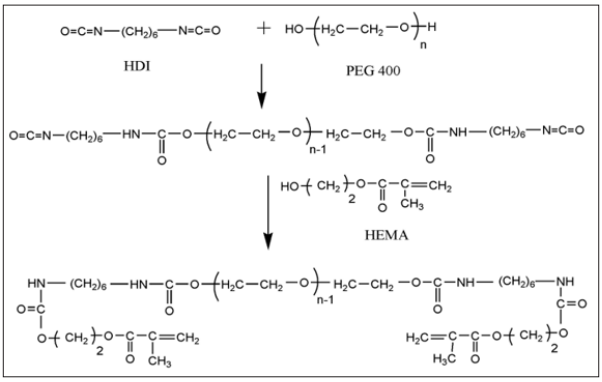

Figure 1: Synthetic scheme of HDI based PUMA.

Curing studies

Initially, AIBN (1% w/w) was dissolved in MMA (15g) and it was added to the pre-polymer with constant stirring. The ratio of pre-polymer and MMA was in the range of 50:50 (by weight) and kept constant in all the nanocomposites. The reaction mixture was then degassed under vacuum for 15min. The resulting mixture was poured into a glass mould having a dimension of 310x220mm and the thickness of the sheet was controlled using 3mm gasket. Glass mould was kept at 60 °C in a water bath for 24h. Post-curing was carried out at 80 °C for 2h in an air oven. The obtained nanocomposite sheets were smooth, transparent and free from wrinkles and voids.

Testing and characterization

FT-IR spectra were recorded at room temperature using a Thermo Scientific Nicolet 6700 FT-IR spectrometer on a diamond disc in the range of 4000-400cm^{-1}. Water absorption was measured as per ASTM D570. Chemical resistance of the nanocomposites was carried out as per ASTM D543. The densities of the nanocomposites were determined as per ASTM D729 using Mettler Toledo instrument. Wide-Angle X-Ray Diffraction (WAXD) measurements for nanocomposites were carried out using an X-ray diffractor unit (Shimadzu Lab XRD-6000) with CuK$_\alpha$ radiation (40kV, 30mA) at a wavelength of 1.54 Å. Shore D hardness was measured as per ASTM D2240 using a durometer. Dumbbell-shaped tensile specimens with a dimension of 165x12.7x3mm were tested using Universal Testing Machine (UTM, AG-IS Shimadzu Lab, 50 kN) as per ASTM D638. A crosshead speed of 50mm/min and a gauge length of 50mm were used for the tensile test. Rectangular bar of 125x12.4x3mm dimension was used for the flexural test using UTM (Instron 3382, 100kN) in accordance with ASTM D790. Three-point bending mode with crosshead speed of 5mm/min and a span length of 100mm were used for carrying out the test. According to ASTM D256, the impact test was carried out using the impact meter 6545 (CEAST, Italy AQ 18). Rectangular bar specimen of 63.5x12.7x3mm dimension with a V-notch depth of 2.54mm and a notch angle of 45° was used for the determination of impact strength. Five samples were tested, and the average was taken for tensile, flexural and impact properties. Abrasion resistance was determined as per ASTM D1044 using Taber Abrader (tmi Testing Machines USA, Model 503 Standard Abrasion tester) and Calibrase CS10F wheel and 1kg load and is reported as weight loss in milligram per 1000 cycles. Wear evaluation study for the abraded surfaces after abrasion testing was investigated using a Carl Ziess SMT (EVO MA15) scanning electron microscope with high tension voltage of 20kV. The samples were conditioned for 1h and sputter coated with gold before imaging. Thermal stability of nanocomposites in the temperature range of 50-600 °C was evaluated using a Perkin Elmer Pyris 7 TGA at a heating rate of 10 °C/min in a nitrogen atmosphere.

Results and Discussion

In our study, *in situ* polymerization technique was used to prepare PUMA/nanoCaCO$_3$ sheets. Prepared nanocomposite sheets ranged from transparent to translucent depending upon the nanoCaCO$_3$ content present in polymer matrix.

Fourier transform infrared spectroscopy

FT-IR spectroscopy was used to confirm the formation of pre-polymer and presence of $CaCO_3$ in nanocomposites. In FT-IR spectrum, absence of isocyanate stretching peak (υ_{NCO}) of HDI at 2250cm^{-1} and broad hydroxyl peak of PEG 400 at 3300cm^{-1}, which confirmed the formation of pre-polymer. υ_{NH} stretching at 3327cm^{-1} indicated the formation of urethane linkage. The absence of $\upsilon_{c=c}$ at 1636cm^{-1} in the FT-IR spectrum of NC-0 indicated that the polymerization had taken place (Figure 2a). In NC-2.0, FT-IR peaks at 1449 and 873cm^{-1} were assigned to carbonate (CO_3^{2-}) of nano$CaCO_3$ particles. Specific absorption peak of CO_3^{2-} at 1449cm^{-1} was found to be broadened due to the interaction between PUMA and nano$CaCO_3$ (Figure 2b). Similar observations were reported for PMDI based PUMA/$CaCO_3$ nanocomposites [31].

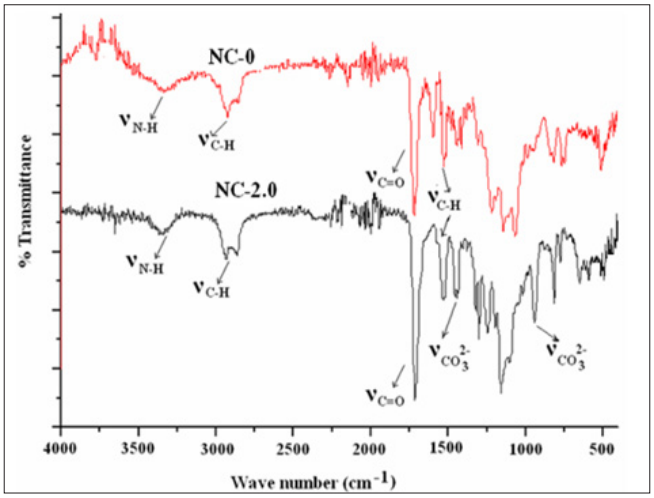

Figure 2: FT-IR spectra of (a) NC-0 and (b) NC-2.0.

Water absorption

As per the ASTM D570, dried and pre-weighed nanocomposite samples were immersed in double distilled water for 24 hours at ambient temperature. Then the surface of the samples was gently wiped and weighed. Water absorption of the samples was measured using the following equation,

$$Water\ absorption(\%) = \frac{W_W - W_D}{W_D} \times 100 \qquad (1)$$

where, W_w and W_D is the wet and dry weight of the samples respectively. The water absorption values of the nanocomposites are shown in Table 1. Water absorption of the nanocomposites increased linearly from 1.37 to 3.53% with respect to nano$CaCO_3$ content in PUMA matrix. The increase in water absorption was attributed to the hydrophilic nature of nano$CaCO_3$ present in PUMA matrix. The hydrophilic nature of $CaCO_3$ might have facilitated the water absorption of nanocomposites.

Table 1: Percentage water absorption, hardness, impact strength and abrasion weight loss of PUMA/$CaCO_3$ nanocomposites.

Composite	Nano $CaCO_3$ (Wt.%)	%Water Absorption	Hardness (shore D)	Izod Impact Strength (J/m)	Abrasion Wt. Loss (mg/1000 cycles)
NC-0	0	1.37	78	32	365
NC-0.5	0.5	1.56	82	26	327
NC-1.0	1	1.96	83	23	312
NC-1.5	1.5	3.23	85	23	211
NC-2.0	2.0	3.53	87	23	190

Chemical resistance

As per ASTM D543, chemical resistance test was carried out for 100 hours at ambient temperature. PUMA and nanocomposite samples were immersed in solvents such as tetrahydrofuran, dimethylformamide, dimethylsulfoxide, acetone and toluene (1% (w/v)). It was found that the samples swelled in all solvents, indicated that they were cross-linked. The nanocomposite samples were also found to be chemically resistant to 1N solution of acids and bases such as HCl, HNO_3, H_2SO_4 and NaOH.

Density

The density of the nanocomposites reflects tightness of microstructure, which can be determined by the specific volume (υ). Under ideal state the density of the nanocomposites (υ_{mix}) can be calculated with the following equation,

$$\rho_{mix} = \frac{m_{mix}}{\upsilon_{mix}} = \frac{m_{mix}}{\frac{m_1}{\rho_1} + \frac{m_2}{\rho_2}} = \frac{1}{\frac{m_1}{m_{mix}\rho_1} + \frac{m_2}{m_{mix}\rho_2}} \qquad (2)$$

Simplified form of this equation is as follows,

$$\frac{1}{\rho_{mix}} = \frac{\frac{m_1}{m_{mix}}}{\rho_1} + \frac{\frac{m_2}{m_{mix}}}{\rho_2} \quad (3)$$

The specific volume of the nanocomposites (υ_{mix}) is based on the density and the content of the nanofiller in the nanocomposites.

$$\upsilon_{mix} = \frac{1}{\rho_{mix}} = \frac{W_1}{\rho_1} + \frac{W_2}{\rho_2} \quad (4)$$

Where ρ_1 and w_1 are the density and weight fraction of PUMA, respectively; ρ_2 and w_2 are the density and weight fraction of nanoCaCO$_3$ respectively. Densification of nanocomposites can be calculated using the following equation,

$$\Delta\upsilon = \left(\upsilon - \upsilon_{mix}\right)$$

where, υ is calculated from density, which is measured by Archimede's principle. Table 2 shows the density values of PUMA/CaCO$_3$ nanocomposites. Densities of the nanocomposites increased with an increase in the nanoCaCO$_3$. The Δυ as difference between the theoretical and experimental values of specific volume are given in Table 2. Negative Δυ value indicated that the structure of the nanocomposites is in condensed form and positive value for loose microstructure. In all the nanocomposite samples, Δυ value is positive which indicated a loose microstructure of nanocomposites. The formation of loose microstructure is attributed to the presence of flexible methylene units in the diisocyanate and glycol moieties.

Table 2: Specific volume of PUMA/CaCO$_3$ nanocomposites.

Sample Code	Density (g/cm^3)	Theoretical ν_{mix} (ml/g)	Experimental ν (ml/g)	Δν (ml/g)
NC-0	1.184	-	0.8445	-
NC-0.5	1.193	0.8341	0.8382	0.0041
NC-1.0	1.196	0.8324	0.8361	0.0037
NC-1.5	1.201	0.8279	0.8326	0.0047
NC-2.0	1.210	0.8182	0.8264	0.0082

WAXD

Wide angle X-ray diffraction analysis exhibited the presence of nanoCaCO$_3$ in polymer matrix. The XRD patterns of NC-0 and NC-2.0 are shown in Figure 3. PUMA exhibited amorphous form, which is indicated by the broad amorphous halo peak at about 20°. The peak at around 30° in NC-2.0 confirmed their incorporation of nanoCaCO$_3$ in polymer matrix. The primary peak that appeared at 30° confirmed that CaCO$_3$ is of calcite type. The absence of peak at 2θ=26.2° and 38.9°, respectively, suggested that nanoCaCO$_3$ is not of aragonite and vaterite type [32].

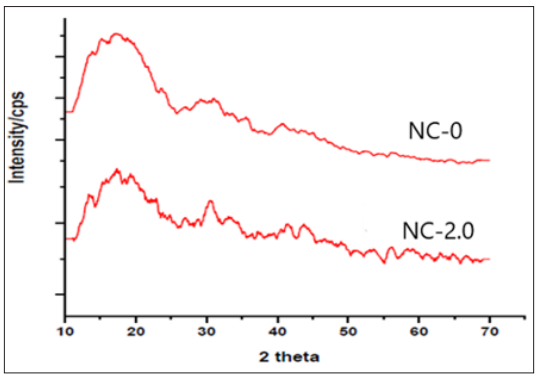

Figure 3: X-ray diffraction pattern of (a) NC-0 and (b) NC-2.0.

Hardness

Shore D hardness values of the PUMA/nanoCaCO$_3$ composites are given in Table 1. Hardness values increased with increase in nanoCaCO$_3$ content, indicating the rigidity of nanocomposites had enhanced. Increase in hardness of PUMA nanocomposites indicated that the interaction between PUMA and nanoCaCO$_3$ increased. This was attributed to the presence of rigid CaCO$_3$ filler in the soft PUMA matrix.

Mechanical properties of PUMA/nanoCaCO$_3$ composites

The mechanical properties of nanocomposites depend to a greater extent upon the uniform distribution of nanofiller in matrix and interfacial morphology such as interfacial structure and interfacial adhesion between filler and matrix as well as stress distribution. Tensile stress-strain curves indicated that the tensile strength increased with increase in nanoCaCO$_3$ percentage, but elongation-at-break decreased in all nanocomposites compared to virgin PUMA matrix (Figure 4). This indicated that the presence of flexible methylene and glycol units in diisocyanate accounted for the higher elongation-at-break for virgin PUMA matrix, but nanocomposites restricted the motion of elongation due to higher molecular interaction between matrix and nanoCaCO$_3$. Elongation-at-break decreased from 20 to 16.1% upon introduction of nanoCaCO$_3$, indicating the reduction in toughness.

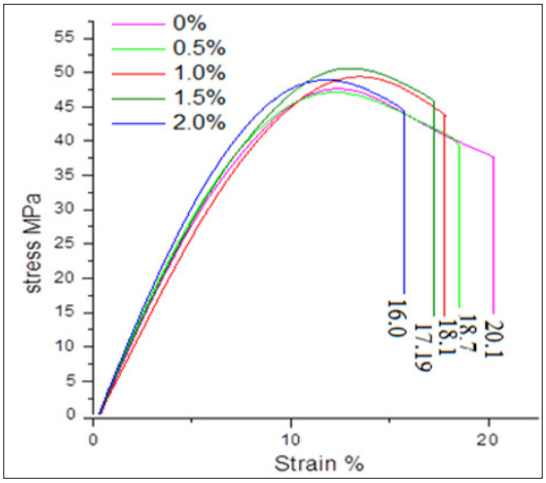

Figure 4: Stress-strain curve of PUMA/CaCO3 nanocomposites.

Tensile strength and modulus

Tensile strength and tensile modulus values for nanocomposite samples are given in Figure 5. Interaction between nanoCaCO$_3$ particles and polymer matrix significantly affects the tensile properties. Introduction of nanoCaCO$_3$ into PUMA matrix enhanced both the tensile strength and modulus. Both tensile strength and modulus of nanocomposites increased substantially with increase in nanoCaCO$_3$ than pristine polymer. Increase in tensile properties indicated that the interaction between nanoCaCO$_3$ particles and polymer matrix is strong. This interaction of nanoCaCO$_3$ with PUMA matrix restricts the movement of molecules upon force, results higher tensile value.

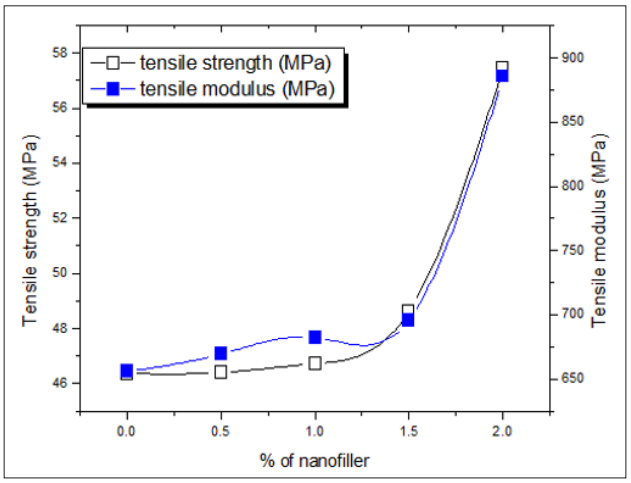

Figure 5: Tensile strength and modulus of PUMA/CaCO$_3$ nanocomposites.

Flexural strength and modulus

The effect of nanoCaCO$_3$ content on flexural strength and flexural modulus are shown in Figure 6. Flexural modulus is an important parameter for measuring the flexural stiffness of materials. It is evident from the (Figure 6), that the flexural properties of the PUMA nanocomposites increased substantially with increase in nanoCaCO$_3$. This behavior was due to the rigidity and reinforcing effect of nanoCaCO$_3$, increased the stiffness results increases the withstand ability upon bending force.

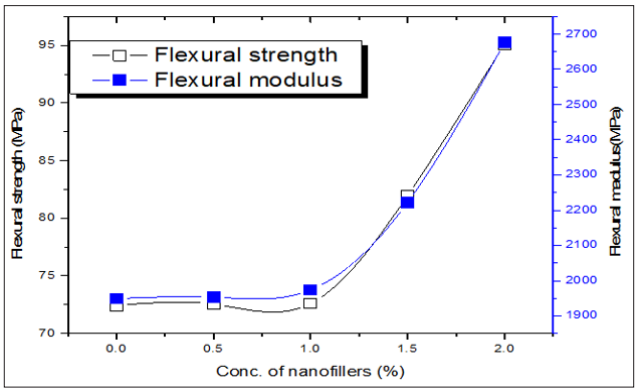

Figure 6: Flexural strength and modulus of PUMA/CaCO$_3$ nanocomposites.

Impact strength

Effect of nanoCaCO$_3$ on the impact strength of PUMA composite values are given in Table 1. Toughness of a material is indicated by the value of its impact strength. Higher the values better the impact strength. NanoCaCO$_3$ loading decreased the impact strength, which indicated that brittleness increased, and toughness decreased in PUMA matrix. Interaction between nanoCaCO$_3$ particles and PUMA matrix was weak and nano sized particles cannot induce shear yielding of polymer matrix. As a result nanoCaCO$_3$ become the defects of materials and could not toughen the PUMA matrix. This observation was in-line with the effect of nanofiller on the values of Elongation-at-break.

Abrasion resistance

Abrasion resistance values of PUMA nanocomposites are tabulated in Table 1. The progressive removal of material from its surface as a result of mechanical action of rubbing, scraping or erosion is defined as abrasion resistance. Increase in nanoCaCO$_3$ content decreased the weight loss indicating that the abrasion resistance increased. The improvement in abrasion resistance indicated that the nanoCaCO$_3$ support part of the applied load which in turn reduces the penetration into polymer. In PUMA, introduction of nanoCaCO$_3$ increases the resistance towards abrasion.

SEM

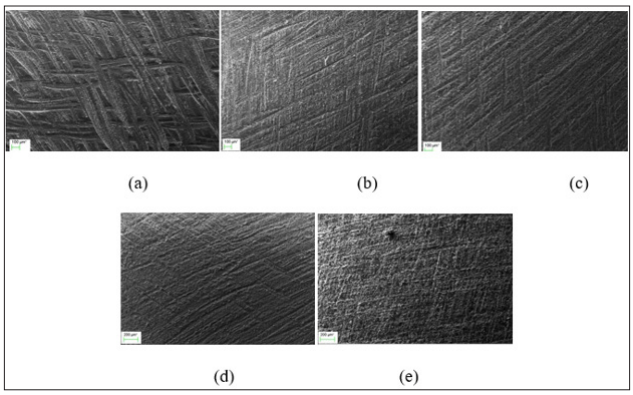

Figure 7: SEM images of abraded surface of (a) NC-0 (b) NC-0.5 (c) NC-1.0 (d) NC-1.5 and (e) NC-2.0.

In order to understand the details of the wear mechanisms operating on each nanocomposite material, SEM was used to probe the morphology of the worn surface (Figure 7). Abrasion occurs mainly by three mechanisms: micro-ploughing, micro-cutting, and micro-cracking [33]. SEM micrographs clearly show the presence of wear marks on the surface along the direction of the flow of wheel. The deep longitudinal lines were observed on the surface are consistent with a repeated ploughing mechanism. This mechanism of ploughing indicted the softness of nanocomposites attributed to the flexible alkyl chain of HDI and PEG. Increasing the content of nanoCaCO$_3$ in PUMA matrix decreased the depth of longitudinal lines indicating that abrasion resistance increased with increase of nanoCaCO$_3$ content. This observation is consistent with abrasion resistance values of nanocomposites.

Thermal stability

Thermal stability of the nanocomposites was evaluated in nitrogen atmosphere using TGA. All the samples were found to be stable in nitrogen atmosphere up to 200 °C and afterwards these samples were found to be two-step degradation (Figure 8). T_{max1} and T_{max2} represents the temperature at which the maximum weight loss occurred in first and second step respectively. Both T_{max1} and T_{max2} increased with increase in nanoCaCO$_3$ indicating that the addition of nanofiller increased the thermal stability of nanocomposites and the extent of increase, increased with increase in nanofiller content on comparison with NC-O. Temperature at which 10, 25, 50 and 75% weight loss occurred for the nanocomposites is given in Table 3. Temperature at specified weight loss increased with increase in nanofiller content. Percentage residue at 600 °C is given in Table 3. Percentage residue increased with increase in nanofiller content. Figure 9 shows a plot of % nanofiller content vs.% residue at 600 °C. This plot can be used to predict the uniform distribution of nanofiller content on PUMA matrix. The correlation factor value of 0.98 indicates that the distribution of nanofiller is uniform and it enhances the thermal stability linearly with increase of nanoCaCO$_3$ in PUMA matrix.

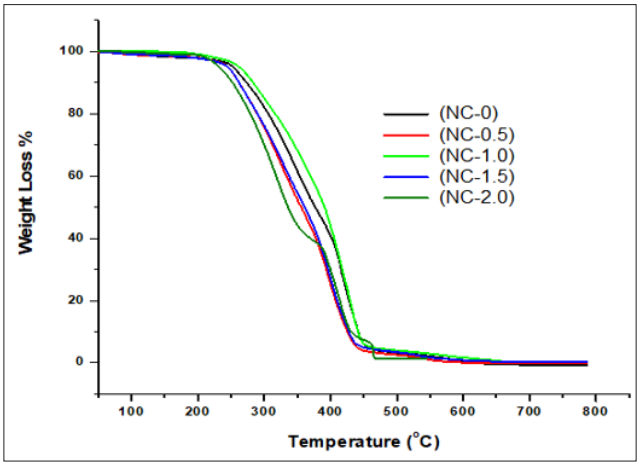

Figure 8: Thermogram of PUMA/CaCO$_3$ nanocomposites under nitrogen atmosphere.

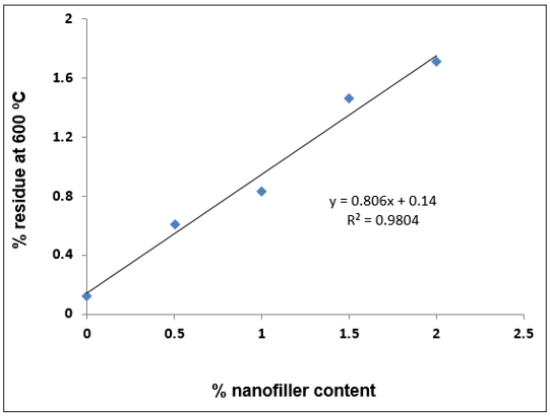

Figure 9: Plot of % nanofiller content vs. % residue at 600 °C.

Table 3: Weight loss of PUMA/CaCO$_3$ nanocomposites upon thermal degradation at different temperature.

Samples	% Weight Loss				% Residue @ 800 °C	T_{max}	
	10%	25%	50%	75%		T_{max1}	T_{max2}
NC-0	251	288	334	399	0.12	328	392
NC-0.5	260	300	354	401	0.61	330	395
NC-1.0	261	302	359	404	0.83	335	399
NC-1.5	273	319	377	421	1.46	339	415
NC-2.0	283	331	390	422	1.71	345	430

Conclusion

PUMA nanocomposites were prepared successfully using HDI, PEG, HEMA and nanoCaCO$_3$. FT-IR spectroscopy and XRD confirmed the incorporation of nanoCaCO$_3$. Tensile strength and modulus, flexural strength and modulus were increased substantially with increase in nanoCaCO$_3$ content. Impact strength decreased with increase in nanoCaCO$_3$ content up to 1.0 wt% and there after it levels off. Density, water absorption, hardness and abrasion resistance increased with increase in nanoCaCO$_3$. Micro ploughing was observed during abrasion wearing of nanocomposites. Two-step thermal degradation was observed in nitrogen atmosphere.

References

1. Maurya SD, Kurmvanshi SK, Mohanty S, Nayak SK (2018) A review on acrylate-terminated urethane oligomers and polymers: Synthesis and applications. Polymer-Plastics Technology and Engineering 57(7): 625-656.
2. Oprea S, Vlad S, Stanciu A (2001) Poly(urethane-methacrylate)s. Synthesis and characterization. Polymer 42(17): 7257-7266.
3. Krishnan PSG, Choudhary V, Varma IK (1993) Current status of urethane methacrylate oligomers and polymers. Journal of Macromolecular Science, Part C Polymer Reviews 33(2):147-180.
4. Paraskar PM, Hatkar VM, Kulkarni RD (2020) Facile synthesis and characterization of renewable dimer acid-based urethane acrylate oligomer and its utilization in UV-curable coatings. Progress in Organic Coatings 149: 105946.

5. Chai KL, Noor IM, Aung MM, Abdullah LC, Kufian MZ (2020) Non-edible oil based polyurethane acrylate with tetrabutylammonium iodide gel polymer electrolytes for dye-sensitized solar cells. Solar Energy 208: 457-468.
6. Khasraghi SS, Shojaei A, Sundararaj U (2019) Bio-based UV curable polyurethane acrylate: Morphology and shape memory behaviors. European Polymer Journal 118: 514-527.
7. Lutz A, Berg OV, Damme JV, Verheyen K, Bauters E, et al. (2015) A shape-recovery polymer coating for the corrosion protection of metallic surfaces. ACS Applied Materials & Interfaces 7(1): 175-183.
8. Alvankarian J, Majlis BY (2012) A new UV-curing elastomeric substrate for rapid prototyping of microfluidic devices. Journal of Micromechanics and Microengineering 22(3): 035006.
9. Schimpf V, Asmacher A, Fuchs A, Bruchmann B, Mülhaupt R (2019) Polyfunctional acrylic non-isocyanate hydroxyurethanes as photocurable thermosets for 3D printing. Macromolecules 52(9): 3288-3297.
10. Liao W, Xu C, Wu X, Xiong Y, Li Z, et al. (2021) A realizable green strategy to negative polyurethane photoresists through the application of a silicone resin photoinitiator. ACS Applied Polymer Materials 3(2): 929-936.
11. Lü C, Cui Z, Wang Y, Li Z, Guan C, et al. (2003) Preparation and characterization of ZnS–polymer nanocomposite films with high refractive index. Journal of Materials Chemistry 13(9): 2189-2195.
12. Zhang H, Tang L, Zhang Z, Gu L, Xu Y, et al. (2010) Wear-resistant and transparent acrylate-based coating with highly filled nanosilica particles. Tribology International 43(1-2): 83-91.
13. López DD, Riquelme RS, Quesada JCG, Gullon IM (2019) Custom-made chemically modified graphene oxide to improve the anti-scratch resistance of urethane-acrylate transparent coatings. Coatings 9: 408
14. Ariffin MM, Aung MM, Abdullah LC, Salleh MZ (2020) Assessment of corrosion protection and performance of bio-based polyurethane acrylate incorporated with nano zinc oxide coating. Polymer Testing 87: 106526.
15. Melinte V, Buruiana T, Balan L, Buruiana EC (2012) Photo-crosslinkable acid urethane dimethacrylates from renewable natural oil and their use in the design of silver/gold polymeric nanocomposites. Reactive and Functional Polymers 72(4): 252-259.
16. Maeda H, Kasuga T (2006) Preparation of poly(lactic acid) composite hollow spheres containing calcium carbonates. Acta Biomaterialia 2(4): 403-408.
17. Jiang L, Lam YC, Tam KC, Chua TH, Sim GW, et al. (2005) Strengthening acrylonitrile-butadiene-styrene (ABS) with nano-sized and micron-sized calcium carbonate. Polymer 46(1): 243-252.
18. Ghalia MA, Inuwa I, Hassan A, Dahman Y (2016) Viscoelastic behavior and mechanical properties of polypropylene/nano-calcium carbonate nanocomposites modified by a coupling agent. Macromolecular Research. doi.org/10.1007/s13233-016-4083-8.
19. Zha L, Fang Z (2010) Polystyrene/$CaCO_3$ composites with different $CaCO_3$ radius and different nano-$CaCO_3$ content-structure and properties. Polymer Composites 31(7): 1258-1264.
20. Bhanvase BA, Gumfekar SP, Sonawane SH (2009) Water-based PMMA-nano-$CaCO_3$ nanocomposites by *in situ* polymerization technique: Synthesis, characterization and mechanical properties. Polymer-Plastics Technology and Engineering 48(9): 939-944.
21. Tang CY, Liang J (2003) A study of the melt flow behaviour of ABS/$CaCO_3$ composites. Journal of Materials Processing Technology 138(1-3): 408-410.
22. Pal MK, Gautam J (2012) Synthesis and characterization of polyacrylamide-calcium carbonate and polyacrylamide-calcium sulfate nanocomposites. Polymer Composites 33(4): 515-523.
23. Nam KH, Seo J, Seo K, Jang W, Han H (2014) Residual stress behavior and physical properties of transparent polyimide/surface-modified $CaCO_3$ nanocomposite films. Macromolecular Research 22(6): 669-677.
24. Jin FL, Park SJ (2008) Thermo-mechanical behaviors of butadiene rubber reinforced with nano-sized calcium carbonate. Materials Science and Engineering: A 478(1-2): 406-408.
25. He H, Li K, Wang J, Sun G, Li Y, et al. (2011) Study on thermal and mechanical properties of nano-calcium carbonate/epoxy composites. Materials and Design 32(8-9): 4521-4527.
26. Baskaran R, Sarojadevi M, Vijayakumar CT (2011) Mechanical and thermal properties of unsaturated polyester/calcium carbonate nanocomposites. Journal of Reinforced Plastics and Composites 30(18):1549-1556.
27. Pundir A, Krishnan PSG, Nayak SK (2017) Effect of nano-calcium carbonate content on the properties of PLA nanocomposites. Journal of Composites and Biodegradable Polymers 5: 26-33.
28. Fujihara K, Kotaki M, Ramakrishna S (2005) Guided bone regeneration membrane made of polycaprolactone/calcium carbonate composite nano-fibers. Biomaterials 26(19): 4139-4147.
29. Gong J, Liu T, Song D, Zhang X, Zhang L (2009) One-step fabrication of three-dimensional porous calcium carbonate–chitosan composite film as the immobilization matrix of acetylcholinesterase and its biosensing on pesticide. Electrochemistry Communications 11(10): 1873-1876.
30. Zuo M, Lai ZZ, Song YH. Zheng Q (2008) Preparation and properties of gluten/calcium carbonate composites. Chinese Chemical Letters 19(8): 992-995.
31. Maurya SD, Purushothaman M, Krishnan PSG, Nayak SK (2014) Effect of nano-calcium carbonate content on the properties of poly(urethane methacrylate) nanocomposites. Journal of Thermoplastic Composite Materials 27(12): 1711-1727.
32. Bang JH, Song KS, Lee MG, Jeon CW, Jang YN (2010) Effect of critical micelle concentration of sodium dodecylsulfate dissolved in calcium and carbonate source solutions on characteristics of calcium carbonate crystals. Materials Transactions 51(8): 1486-1489.
33. Cenna AA, Doyle J, Page NW, Beehag A, Dastoor P (2000) Wear mechanisms in polymer matrix composites abraded by bulk solids. Wear 240(1-2): 207-214.